

# Seeded strain-like transmission of $\beta$ -amyloid morphotypes in APP transgenic mice

Götz Heilbronner<sup>1,2</sup>, Yvonne S. Eisele<sup>1,2</sup>, Franziska Langer<sup>1,2</sup>, Stephan A. Kaeser<sup>1,2</sup>, Renata Novotny<sup>1,2,3</sup>, Amudha Nagarathinam<sup>1,2</sup>, Andreas Åslund<sup>4</sup>, Per Hammarström<sup>4</sup>, K. Peter R. Nilsson<sup>4</sup> & Mathias Jucker<sup>1,2+</sup>

<sup>1</sup>Department of Cellular Neurology, Hertie Institute for Clinical Brain Research, University of Tübingen, Tübingen, Germany, <sup>2</sup>DZNE, German Center for Neurodegenerative Diseases, Tübingen, Germany, <sup>3</sup>Graduate School of Cellular and Molecular Neuroscience, University of Tübingen, Tübingen, Germany, and <sup>4</sup>Department of Chemistry, IFM, Linköping University, Linköping, Sweden

The polymorphic  $\beta$ -amyloid lesions present in individuals with Alzheimer's disease are collectively known as cerebral  $\beta$ -amyloidosis. Amyloid precursor protein (APP) transgenic mouse models similarly develop  $\beta$ -amyloid depositions that differ in morphology, binding of amyloid conformation-sensitive dyes, and A $\beta$ 40/A $\beta$ 42 peptide ratio. To determine the nature of such  $\beta$ -amyloid morphotypes,  $\beta$ -amyloid-containing brain extracts from either aged APP23 brains or aged APPPS1 brains were intracerebrally injected into the hippocampus of young APP23 or APPPS1 transgenic mice. APPPS1 brain extract injected into young APP23 mice induced  $\beta$ -amyloid deposition with the morphological, conformational, and A $\beta$ 40/A $\beta$ 42 ratio characteristics of  $\beta$ -amyloid deposits in aged APPPS1 mice, whereas APP23 brain extract injected into young APP23 mice induced  $\beta$ -amyloid deposits with the characteristics of  $\beta$ -amyloid deposits in aged APP23 mice. Injecting the two extracts into the APPPS1 host revealed a similar difference between the induced  $\beta$ -amyloid deposits, although less prominent, and the induced deposits were similar to the  $\beta$ -amyloid deposits found in aged APPPS1 hosts. These results indicate that the molecular composition and conformation of aggregated A $\beta$  in APP transgenic mice can be maintained by seeded conversion.

Keywords: Alzheimer; amyloid; protein aggregation; prion strain

EMBO reports (2013) 14, 1017–1022. doi:10.1038/embor.2013.137

## INTRODUCTION

The aggregation and deposition of the  $\beta$ -amyloid peptide (A $\beta$ ) in brain is considered an early and predictive lesion of Alzheimer's disease (AD) [1–3]. A $\beta$  of various lengths are generated by cleavage of amyloid precursor protein (APP) by  $\beta$ -secretase and  $\gamma$ -secretase [4,5]. The most prominent A $\beta$  species are full-length or N-truncated A $\beta$ x-40 (A $\beta$ 40) and A $\beta$ x-42 (A $\beta$ 42) with A $\beta$ 42 being much more prone to aggregation and more neurotoxic compared with A $\beta$ 40 [4,5].

There are multiple lines of evidence for polymorphic A $\beta$  aggregation [6,7]. A $\beta$  deposits in brain can differ in morphology and in biochemical composition within and among individuals with AD, between normal aging and AD, and among APP transgenic mouse models [6–13]. Such A $\beta$  morphotypes might be governed by host factors, such as A $\beta$  posttranslational modifications, A $\beta$  length variant generation or A $\beta$  amino-acid substitutions as found in familial AD. However, we have previously shown the induction of different A $\beta$  morphotypes in a given transgenic mouse line after intracerebral application of aggregated A $\beta$ -containing brain extracts from two different sources [14]. Similarly, *in vitro*, distinct structural variants of synthetic A $\beta$  fibrils can be grown and are self-propagating under seeded growth conditions [15,16].

The aim of the present study was to determine whether the induction of different A $\beta$  morphotypes in genetically defined recipient mice reflect variations in the molecular composition and/or conformation of the aggregated A $\beta$  in the donor brain extracts. This would suggest that the prion conformation strain concept [17–20] might also apply to cerebral  $\beta$ -amyloidosis and further supports the concept of prion-like templated misfolding of A $\beta$ .

## RESULTS AND DISCUSSION

### A $\beta$ morphotypes in APP23 and APPPS1 mice

APP23 and APPPS1 transgenic mice develop age-dependent depositions of A $\beta$  in the brain [21,22]. While amyloid deposits in APP23 mice are characterized by fairly large A $\beta$  deposits consisting of congophilic amyloid cores with diffuse penumbras, as well as diffuse A $\beta$  deposition, APPPS1 mice develop small,

<sup>1</sup>Department of Cellular Neurology, Hertie Institute for Clinical Brain Research, University of Tübingen, D-72076 Tübingen, Germany

<sup>2</sup>DZNE, German Center for Neurodegenerative Diseases, D-72076 Tübingen, Germany

<sup>3</sup>Graduate School of Cellular and Molecular Neuroscience, University of Tübingen, D-72074 Tübingen, Germany

<sup>4</sup>Department of Chemistry, IFM, Linköping University, SE-581 83 Linköping, Sweden

+Corresponding author. Tel: +49 7071 29 86863; Fax: +49 7071 29 4521;

E-mail: mathias.jucker@uni-tuebingen.de

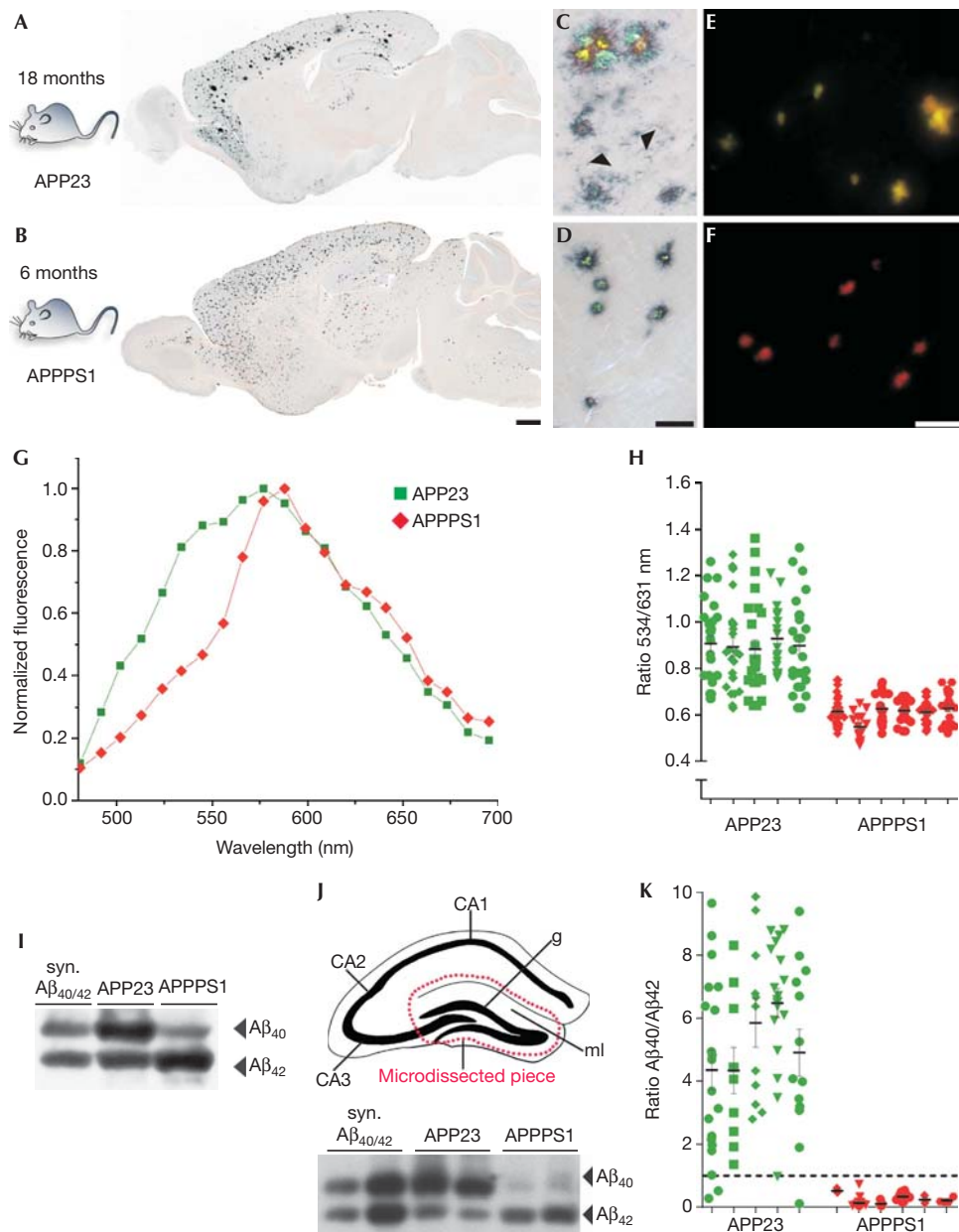


**Fig 1** | A $\beta$  deposits in APP23 and APPPS1 mice differ in morphology, spectral properties and A $\beta$ 40/42 ratio. (A,B) A $\beta$ -immunostaining and Congo red staining of an 18-month-old APP23 and 6-month-old APPPS1 mouse. (C,D) Higher magnification of the hippocampal plaques. Note the rather large congophilic (yellow–green birefringence) plaques and diffuse (arrowheads) A $\beta$  deposits in APP23 mice (C) in comparison with the smaller, compact and congophilic plaques in APPPS1 mice (D). (E,F) tPTAA staining of the hippocampal plaques. Note the shift to yellow–green colours of the A $\beta$  deposits in the 18-month-old APP23 mice (E) and the reddish colour of the deposits in the 6-month-old APPPS1 mice (F). Scale bars, 500  $\mu$ m (B), 100  $\mu$ m (D), 50  $\mu$ m (F). (G) Emission spectra of tPTAA bound to the hippocampal A $\beta$  deposits. (H) For quantitative analysis, the ratio of the intensity of the emitted light at 534 and 631 nm was calculated. Each dot represents one A $\beta$  plaque. Mean and s.e.m. are indicated for each animal. *t*-Test revealed a significant difference between the two groups (APP23: 5 mice, 18–22 months old; APPPS1: 6 mice, 4–6 months old;  $t(9) = 19.4$ ;  $P < 0.001$ ). Note the greater variation between individual plaques within the APP23 mice compared with APPPS1 mice. (I–K) Urea-based immunoblot of amyloid-depositing APP23 and APPPS1 mouse brain (I; lane 1: synthetic A $\beta$ 40 + A $\beta$ 42 (400 pg each), lane 2: APP23 brain extract, lane 3: APPPS1 brain extract). Note the dominance of A $\beta$ 40 over A $\beta$ 42 in APP23 mice and of A $\beta$ 42 over A $\beta$ 40 in APPPS1 mice. Similar results were obtained with laser-dissected tissue pieces from the dentate gyrus (J top; schematic drawing; CA1–3 = cornu ammonis area; g = granular cell layer; ml = molecular layer; J bottom: immunoblot of two laser-dissected tissue pieces from APP23 and APPPS1; synthetic A $\beta$ 40 + A $\beta$ 42 were 400 and 800 pg each). Quantitative densitometric A $\beta$ 40/A $\beta$ 42 ratio in immunoblots for each laser-dissected tissue piece (K, for each animal between 3 and 28 sections were analysed and are represented by dots). The dotted line indicates a ratio of 1. The same 5–6 mice/group were used as in (H). Mean and s.e.m. are indicated. *t*-Test revealed a significant difference between the two groups ( $t(9) = 11.5$ ;  $P < 0.001$ ). A $\beta$ ,  $\beta$ -amyloid peptide; tPTAA, trimeric polythiophene acetic acid.

compact and highly congophilic A $\beta$  deposits [21,22]. These mouse strain-specific plaque morphotypes can be found throughout the neocortex and hippocampus (Fig 1A–D).

Conformational differences of variant A $\beta$  morphotypes can be studied by anionic luminescent conjugated polythiophene (LCP) including trimeric polythiophene acetic acid (tPTAA) [23]. LCPs are flexible amyloid-binding dyes whose spectral properties depend on the amyloid conformation. An LCP-based histo-optical imaging technique has previously been used to discriminate various prion strains, types of systemic amyloids and heterogeneous A $\beta$  deposits [12,24,25]. When tPTAA was applied to tissue sections of amyloid-bearing APP23 and APPPS1 mice, fluorescence images revealed a shift towards bright yellow–greenish colours for the amyloid plaques in APP23 mice, whereas the amyloid plaques in APPPS1 mice showed a reddish appearance (Fig 1E,F). Subsequent spectral analysis revealed tPTAA emission spectra in APP23 mice with a maximum intensity at  $\sim$ 575 nm and a shoulder at shorter wavelengths (around 535 nm), with more red-shifted spectra also present (Fig 1G). In contrast, plaques in the APPPS1 mice showed a narrower tPTAA spectral distribution with a maximum intensity at  $\sim$ 590 nm and a shoulder at longer wavelengths (around 630 nm) (Fig 1G). Quantitative results revealed a significant difference in the 534/631 nm emission ratio between the amyloid deposits in APP23 and APPPS1 mice (Fig 1H; see also supplementary Fig S1 online). The spectral difference was also present, albeit less distinct, when amyloid fibrils were isolated from whole brains of APP23 and APPPS1 mice (supplementary Fig S2 online).

APP23 mice express Swedish-mutated human APP, with A $\beta$ 40 generation exceeding that of A $\beta$ 42. In contrast, APPPS1 mice harbour mutated presenilin (PS) 1 in addition to Swedish-mutated APP, and thus generate more A $\beta$ 42 than A $\beta$ 40 albeit lower total amounts of total A $\beta$  compared with APP23 mice [21,22]. To test whether this difference in A $\beta$  length variant generation is also reflected in the amyloid plaques, laser dissection of amyloid plaques with subsequent A $\beta$ -immunoblotting was performed. Results revealed an A $\beta$ 40/42 ratio of 4.7/1 for aged APP23 mice, and a ratio of 0.3/1 for APPPS1 mice (Fig 1I–K) consistent with enzyme-linked immunosorbent assays from brain homogenates [14,21,22].

### Propagation of A $\beta$ morphotypes by seeding

Intracerebral injection of minute amounts of brain extract from  $\beta$ -amyloid-laden aged APP23 or APPPS1 mice induces  $\beta$ -amyloidosis in young pre-depositing APP23 and APPPS1 mice [14]. Here we have replicated these findings and show that  $\beta$ -amyloid-containing APP23 extract injected into the hippocampus (dentate gyrus) of young, pre-depositing, 4–6-month-old APP23 mice induces  $\beta$ -amyloid deposits surrounded by diffuse, filamentous A $\beta$  immunoreactivity 3 months after injections. In contrast,  $\beta$ -amyloid-containing APPPS1 extract injected in the same host induces punctate, coarse and compact A $\beta$ -plaques 3 months after injections (Fig 2A–C). While the APP23 extract induced A $\beta$  deposits throughout the subgranular and molecular layers of the dentate gyrus, the induced A $\beta$  deposits by the APPPS1 extract were largely confined to the subgranular layer and polymorphic region of the dentate gyrus (Fig 2B,C). Quantification revealed that total A $\beta$  deposition induced by the APP23 extract was more than double compared with the

APPPS1 extract (Fig 2B,C). In contrast, when only the compact A $\beta$  deposition was quantified, there was no clear difference between the two extracts (Fig 2B,C).

The reverse experiment, that is, APP23 and APPPS1 extracts injected into young, pre-depositing 1.5–3-month-old APPPS1 mice and analysed 1.5–3 months later, revealed again a more diffuse and filamentous pattern of A $\beta$ -deposition for the APP23 extract and prominent A $\beta$ -deposition in the subgranular cell layer for the APPPS1 extract. However, this morphological difference between the extracts was not as obvious as in the APP23 host and also the induced amount and pattern of total or compact A $\beta$  immunoreactivity appeared similar between the two extracts (Fig 2D,E).

APP23 and APPPS1 mice analysed 1 week after the injection of the  $\beta$ -amyloid-containing brain extracts did not show amyloid deposition demonstrating that the A $\beta$  deposits did not simply represent the injected A $\beta$ -containing material ( $n=8$ ; 2 mice/group; results not shown) [14,26].

### tPTAA spectral emission of seeded A $\beta$ deposits

To study conformational differences of the induced A $\beta$  morphotypes, tPTAA staining with spectral analysis was applied (Fig 2F–I). Strikingly, while the APP23 extract injected in APP23 mice induced A $\beta$  deposits with a yellow–greenish appearance, the APPPS1 extract injected in APP23 mice induced A $\beta$  deposits with a reddish shifted appearance (Fig 2F,G). Vice versa, while the A $\beta$  deposits in APP23 extract-seeded APPPS1 mice revealed a spectral shift towards a yellow–greenish colour, the APPPS1 extract-seeded APPPS1 mice revealed a more reddish pattern, although this difference appeared again less striking compared with the APP23 host (Fig 2H,I). Quantitative spectral analysis of the 534/631 nm emission ratio confirmed this qualitative histological impression (Fig 3A). When compared with the endogenous A $\beta$  deposits of the hosts (Fig 1H), the 534/631 nm emission ratios in APP23-seeded APP23 mice and APPPS1-seeded APPPS1 mice were reminiscent of the emission ratios in APP23 and APPPS1 mice, respectively.

### A $\beta$ 40/42 ratio of seeded A $\beta$ deposits

To test whether the ratio of A $\beta$ 40/42 might underlie the different morphology and LCP spectral analysis of the induced A $\beta$  deposits, laser dissection of induced A $\beta$  deposition with subsequent A $\beta$ -immunoblotting was performed (Fig 3B). Intriguingly, there was a significant difference between APP23-seeded and APPPS1-seeded A $\beta$  deposits in the APP23 host. While APP23-seeded A $\beta$  deposits showed a mean A $\beta$ 40/42 ratio of 3.7/1, APPPS1-seeded APP23 mice revealed a mean A $\beta$ 40/42 ratio of 1.5/1. (Note that in ‘unseeded’ APP23 mice, the ratio was 4.7/1 and in APPPS1 mice 0.3/1, see Fig 1K). This finding implies the existence of a selection mechanism, whereby the seeded A $\beta$  deposits incorporate mainly the host-generated A $\beta$  isoform that resembles the composition of the seed. This seeded imprinting of the A $\beta$ 40/42 ratio in the APP23 host paralleled the morphological characteristics of the induced A $\beta$  deposits and LCP staining.

In the APPPS1 host and in contrast to the LCP staining, immunoblot analysis of the induced A $\beta$  deposition failed to reach significance between the two extracts (A $\beta$ 40/42 ratio of 0.35/1 for APP23 extract versus 0.25/1 for APPPS1 extract; Fig 3B) and the ratios of both APP23- and APPPS1-seeded A $\beta$  deposits were

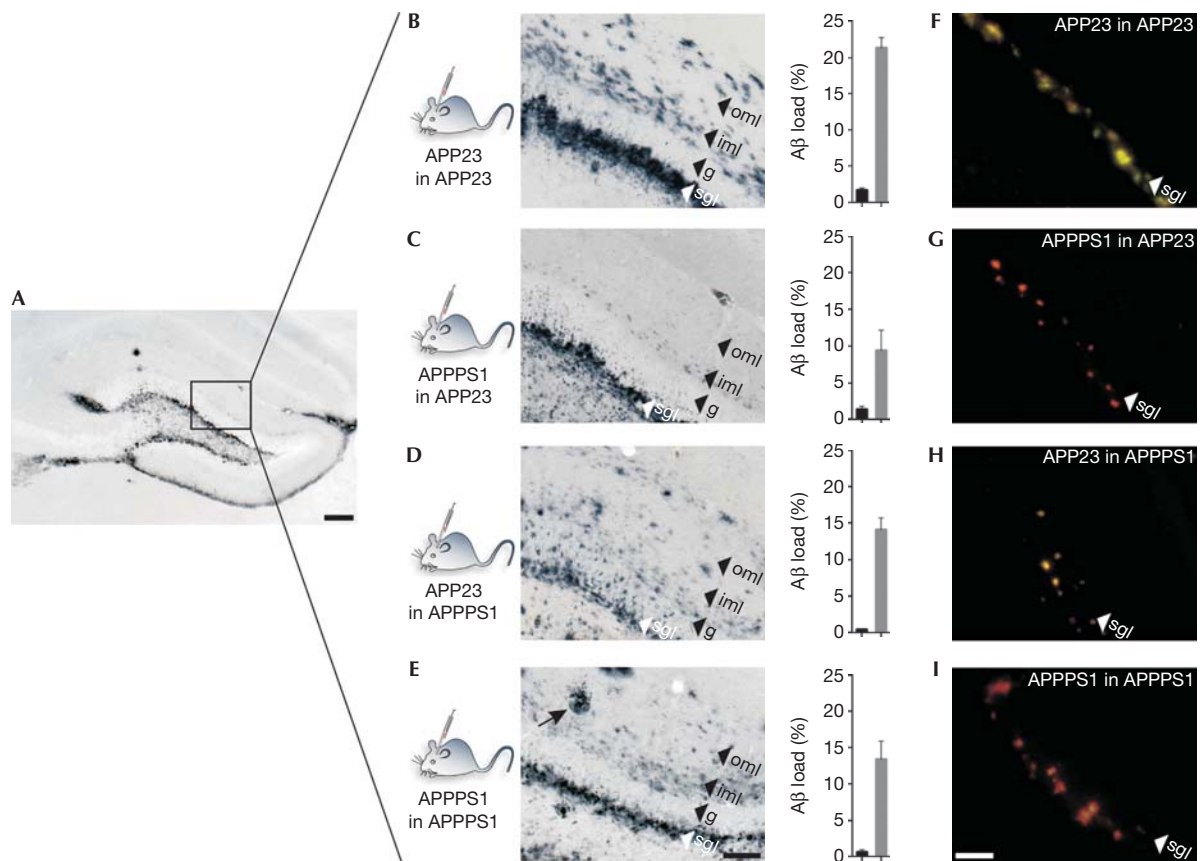


**Fig 2** | Propagation of A $\beta$  morphotypes by seeding. Brain extracts from aged amyloid-depositing APP23 or APPPS1 mice were injected into the hippocampus (dentate gyrus) of APP23 or APPPS1 mice. APP23 mice were 4–6 months old when they were injected. They were analysed 3 months later ( $n = 5$ /extract). APPPS1 mice were either 1.5–2 months or 3 months old when they were injected. The 1.5–2-month-old group was analysed 1.5–2 months later ( $n = 6$ /extract). The 3-month-old group was analysed 3 months later ( $n = 2$ /extract). (A) Pattern of induced A $\beta$ -deposition (A $\beta$  immunostaining) in the dentate gyrus. Shown is an APPPS1 extract-inoculated APPPS1 host. (B–E) Higher magnifications of A $\beta$ -immunostained layers of the dentate gyrus for the four experimental groups. The APP23 extract-induced A $\beta$  deposits in APP23 hosts are more diffuse and filamentous compared with the highly coarse, punctate and compact A $\beta$  deposits in APPPS1 extract-induced APP23 hosts (B,C). The distribution of the induced A $\beta$  deposits throughout the different layers was also different between the two extracts in the APP23 host (sgl = subgranular cell layer; g = granular cell layer; iml, oml = inner and outer molecular layer). In the APPPS1 host, the APP23 extract-induced A $\beta$ -deposits also appeared somewhat more diffuse and filamentous compared with the APPPS1 extract-induced A $\beta$ -deposits, whereas the APPPS1 extract induced again more prominent A $\beta$ -deposition in the sgl compared with the APP23 extract (D,E). Overall, the morphological differences between the two extracts in the APPPS1 host were less obvious than in the APP23 host and this appeared true independent of the age of the host at the time of inoculation and of the inoculation period. Note that untreated APP23 mice at 7–9 months of age do not yet show endogenous A $\beta$  plaques in the hippocampus whereas APPPS1 mice at 4–6 months of age occasionally have some endogenous hippocampal plaques, which however can easily be identified (arrowhead in E). Total A $\beta$  load (grey bars) and compact A $\beta$  load (black bars) in dentate gyrus is shown in the panels next to the histological panels. Mean and s.e.m. are indicated (for the APP23 host  $n = 5$ /extract, for the APPPS1 host  $n = 8$ /extract). ANOVA (extract  $\times$  host) for the A $\beta$  load revealed a significant interaction  $F(1,22) = 6.19$ ;  $P < 0.05$  and a significant main effect for extract ( $F(1,22) = 7.78$ ;  $P < 0.05$ ) but not for host ( $P > 0.05$ ). ANOVA for the compact A $\beta$  revealed a significant main effect for host ( $F(1,22) = 10.12$ ;  $P < 0.01$ ) but not for extract or interaction ( $P > 0.05$ ). (F–I) tPTAA stained dentate gyrus for the four experimental groups. Note the difference in colour between the APP23 extract-induced A $\beta$  deposits (yellow–greenish, F) and the APPPS1 extract-induced A $\beta$  deposits (yellow–reddish, G) in APP23 hosts. The difference between the two extract in the APPPS1 host was again somewhat less prominent (H, I). Scale bars, 200  $\mu$ m (A), 100  $\mu$ m (E) and 50  $\mu$ m (I). A $\beta$ ,  $\beta$ -amyloid peptide; ANOVA, analysis of variance; tPTAA, trimeric polythiophene acetic acid.

similar to ratio in the ‘unseeded’ APPPS1 host. This observation might reflect that seeded nucleation in the APPPS1 host was obscured by endogenous spontaneous nucleation events and/or cross-seeding of the abundant and highly aggregate-prone A $\beta$ 42 generated by the APPPS1 host [6,22].

### ‘Strain-like’ A $\beta$ morphotypes

Prion strains might differ in amino-acid sequence of the prion protein or are based on polymorphic assembled states of the same prion protein molecule [17–20]. While the latter has at least been shown for A $\beta$  *in vitro* [15,16], the results of the present study

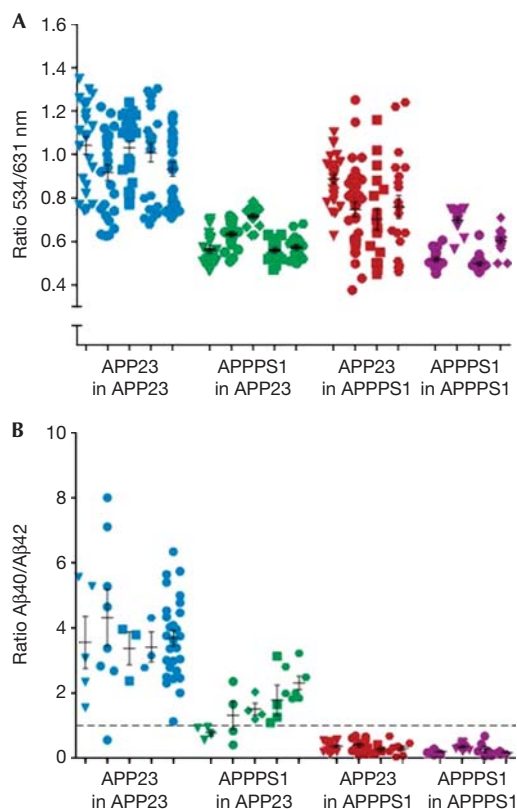


**Fig 3** | Quantitative tPTAA spectral emission and A $\beta$ 40/42 ratio of induced A $\beta$  deposits. The analysis is from the same mice as in Fig 2. For the APP23 host, all mice ( $n = 5$ /extract) were included in the analysis; for the APPPS1 host, the two extremes were selected for analysis, that is, the 1.5-month-old mice that were analysed 1.5 months later, and the 3-month-old mice that were analysed 3 months later (total  $n = 4$ /extract). (A) Quantitative emission spectra of the ratio of the emitted light at 534 nm and 631 nm. For methodological details see Fig 1. Mean and s.e.m. are indicated. ANOVA (host  $\times$  extract) revealed significant main effects (host  $F(1,14) = 12.0$ ;  $P < 0.01$ ; Extract  $F(1,14) = 67.1$ ;  $P < 0.001$ ) and interaction ( $F(1,14) = 6.8$ ;  $P < 0.05$ ). *Post hoc* analysis revealed significant differences between APP23- and APPPS1-induced A $\beta$  deposits in the APP23 host ( $P < 0.001$ ) and APPPS1 host ( $P < 0.01$ ). (B) Densitometric analysis of the A $\beta$ 40/A $\beta$ 42 ratio plotted for each laser-dissected tissue piece. For methodological details see Fig 1. Mean and s.e.m. are indicated. The dotted line indicates a ratio of 1. ANOVA (host  $\times$  extract) revealed significant main effects (Host  $F(1,14) = 175.9$ ;  $P < 0.001$ ; extract  $F(1,14) = 40.5$ ;  $P < 0.001$ ) and interaction ( $F(1,14) = 34.41$ ;  $P < 0.001$ ). *Post hoc* analysis revealed a difference between the APP23- and APPPS1-induced A $\beta$  deposits in the APP23 host ( $P < 0.001$ ) but failed to reach significance in the APPPS1 host ( $P > 0.05$ ). A $\beta$ ,  $\beta$ -amyloid peptide; ANOVA, analysis of variance; tPTAA, trimeric polythiophene acetic acid.

suggest that, for  $\beta$ -amyloidosis in brain, C-terminal chain-length variants might contribute to the nature of the A $\beta$  conformers and can be sustained by seeded induction ('strains'). In apparent contrast, previous *in vitro* studies have reported that assemblies of A $\beta$  protofibrils with different A $\beta$ 40/42 ratios have similar molecular structures [27,28]. However, *in vivo* and within

a cellular environment A $\beta$  aggregation is likely different [10]. While the present study only focused on A $\beta$ 40 and A $\beta$ 42, it should be noted that there are many additional A $\beta$  isoforms with various amino- and carboxy terminal lengths. In addition, there are A $\beta$  amino-acid sequence differences associated with familial forms of cerebral  $\beta$ -amyloidosis [5,29].

The physiological relevance of A $\beta$  'strains' and whether they can be linked to phenotypic variability of AD and/or cerebral  $\beta$ -amyloidosis, as reported for prion strains in prionoses [18–20], remains to be shown. However, *in vitro*, the neurotoxicity of A $\beta$  fibrils is dependent on their molecular and structural composition, including their A $\beta$ 40/42 ratio [15,30–32]. *In vivo*, it has been shown that subtle changes in the A $\beta$ 40/42 ratio have profound effects on neurotoxicity [33]. Finally, the A $\beta$ 40/42 ratio correlates with disease onset in familial AD [34,35].

Cerebral  $\beta$ -amyloidosis is likely initiated by stochastic A $\beta$  seed formation, with subsequent propagation and spreading [6,36]. The finding that variants of A $\beta$  seeds might govern the type (and possibly toxicity) of A $\beta$  aggregates might at least partly explain the heterogeneous morphology, pathogenicity and progression of A $\beta$  lesions and associated pathologies in AD. The identification of factors that influence the conformational characteristics of the initial seed might thus have therapeutic implications.

## METHODS

Detailed methods can be found in the Supplementary Information Online.

**Mice and brain extracts.** APP23 and APPPS1 transgenic mice develop first amyloid deposits at 6–8 months (APP23) and 2–4 months (APPPS1) of age. In both strains, A $\beta$  deposits develop first in neocortex and later in the hippocampus [21,22]. Brain extracts were prepared from 27–28-month-old APP23 and 16–22-month-old APPPS1 mice (10–20 ng A $\beta$ / $\mu$ l for both extracts). Injections were done into the hippocampus/dentate gyrus (AP  $- 2.5$  mm, L  $+/- 2.0$  mm, DV  $- 1.8$  mm) [26].

**Immunohistochemistry and stereology.** Sections were stained with Congo red and polyclonal antibody to A $\beta$  [37]. Induced A $\beta$  deposition was quantified on a set of every 12th systematically sampled coronal section throughout the dentate gyrus [14]. Total A $\beta$ -load was determined by calculating the areal fraction (percentage) occupied by A $\beta$ -staining; the compact plaque load by calculating the areal fraction occupied by Congo red.

**tPTAA staining and emission spectra.** Spectra were collected from tPTAA-stained sections [23] with a LSM 780 or 510 META (Carl Zeiss, Jena, Germany) with an argon 488 nm laser, and a Leica DM6000 B fluorescence microscope (Leica, Wetzlar, Germany) equipped with a SpectraCube (optical head) module (Applied Spectral Imaging, Migdal Ha-Emek, Israel). SpectraView 3.0 EXPO software (Applied Spectral Imaging) was used for images and selection of spectral regions. Spectra were collected from eight spots within 15–20 plaques/animal. Twisted separated LCP molecules emit light at 530–540 nm, whereas planar, stacked (aggregated) LCP multimers emit light at 630–650 nm. The ratio of the intensity of the emitted light at 534 and 631 nm was used as a parameter for spectral distinction of different plaques [12].

**Immunoblotting of Laser-Dissected Tissue.** Laser-microdissected (MicroBeam, P.A.L.M., Bernried, Germany) patches of the dentate gyrus (see Fig 1j) were cut from sections adjacent to

A $\beta$ -immunostained sections in which the location of the A $\beta$  induction was confirmed. Bicine-Tris urea SDS-PAGE immunoblotting was used to separate A $\beta$ 40 and A $\beta$ 42 using antibody 6E10 specific to human A $\beta$  [14]. Densitometric values of band intensities were analysed to calculate the A $\beta$ 40:A $\beta$ 42 ratio using ImageJ, version 1.42q (<http://rsb.info.nih.gov/ij>).

**Supplementary information** is available at EMBO reports online (<http://www.emboreports.org>).

#### ACKNOWLEDGEMENTS

We thank Matthias Staufenbiel (Basel) and Lary Walker (Atlanta) for comments to this manuscript; Ulla Welzel, Sarah Fritschi, Uli Obermüller, Claudia Schäfer (Tübingen), and Sofie Nyström (Linköping) for experimental help; Monika Schütz and Ingo Autenrieth (Tübingen) for help with the laser-microdissection. Supported by BMBF (ERA-Net NEURON—MIPROTRAN), European Union FP7 HEALTH (LUPAS), the Swedish Foundation for Strategic Research (SSF), and an ERC starting independent researcher grant (K.P.R.N.).

**Author contributions:** Y.S.E. and M.J. designed the research; G.H., Y.S.E., F.L. S.A.K., R.N., A.Ä., P.H. and K.P.R.N. performed the research; G.H., Y.S.E., A.N., K.P.R.N., P.H. and M.J. analysed data and prepared figures; M.J., K.P.R.N., P.H. wrote manuscript.

#### CONFLICT OF INTEREST

The authors declare that they have no conflict of interest.

#### REFERENCES

- Morris JC, Roe CM, Grant EA, Head D, Storandt M, Goate AM, Fagan AM, Holtzman DM, Mintun MA (2009) Pittsburgh compound B imaging and prediction of progression from cognitive normality to symptomatic Alzheimer disease. *Arch Neurol* **66**: 1469–1475
- Weiner MW et al (2010) The Alzheimer's disease neuroimaging initiative: progress report and future plans. *Alzheimers Dement* **6**: 202–211; e207
- Bateman RJ et al (2012) Clinical and biomarker changes in dominantly inherited Alzheimer's disease. *N Engl J Med* **367**: 795–804
- Haass C, Selkoe DJ (2007) Soluble protein oligomers in neurodegeneration: lessons from the Alzheimer's amyloid beta-peptide. *Nat Rev Mol Cell Biol* **8**: 101–112
- De Strooper B (2010) Proteases and proteolysis in Alzheimer disease: a multifactorial view on the disease process. *Physiol Rev* **90**: 465–494
- Eisenberg D, Jucker M (2012) The amyloid state of proteins in human diseases. *Cell* **148**: 1188–1203
- Levine H 3rd, Walker LC (2010) Molecular polymorphism of Abeta in Alzheimer's disease. *Neurobiol Aging* **31**: 542–548
- Piccini A et al (2005) beta-amyloid is different in normal aging and in Alzheimer disease. *J Biol Chem* **280**: 34186–34192
- Maarouf CL et al (2008) Histopathological and molecular heterogeneity among individuals with dementia associated with Presenilin mutations. *Mol Neurodegener* **3**: 20
- Paravastu AK, Qahwash I, Leapman RD, Meredith SC, Tycko R (2009) Seeded growth of beta-amyloid fibrils from Alzheimer's brain-derived fibrils produces a distinct fibril structure. *Proc Natl Acad Sci USA* **106**: 7443–7448
- Rosen RF, Ciliax BJ, Wingo TS, Gearing M, Dooyema J, Lah JJ, Ghiso JA, LeVine H 3rd, Walker LC (2010) Deficient high-affinity binding of Pittsburgh compound B in a case of Alzheimer's disease. *Acta Neuropathol* **119**: 221–233
- Nilsson KP et al (2007) Imaging distinct conformational states of amyloid-beta fibrils in Alzheimer's disease using novel luminescent probes. *ACS Chem Biol* **2**: 553–560
- Herzig MC, Eisele YS, Staufenbiel M, Jucker M (2009) E22Q-mutant Abeta peptide (AbetaDutch) increases vascular but reduces parenchymal Abeta deposition. *Am J Pathol* **174**: 722–726
- Meyer-Luehmann M et al (2006) Exogenous induction of cerebral beta-amyloidogenesis is governed by agent and host. *Science* **313**: 1781–1784
- Petkova AT, Leapman RD, Guo Z, Yau WM, Mattson MP, Tycko R (2005) Self-propagating, molecular-level polymorphism in Alzheimer's beta-amyloid fibrils. *Science* **307**: 262–265
- Meinhardt J, Sachse C, Hortschansky P, Grigorieff N, Fandrich M (2009) Abeta(1–40) fibril polymorphism implies diverse interaction patterns in amyloid fibrils. *J Mol Biol* **386**: 869–877
- Jones EM, Surewicz WK (2005) Fibril conformation as the basis of species- and strain-dependent seeding specificity of mammalian prion amyloids. *Cell* **121**: 63–72
- Collinge J, Clarke AR (2007) A general model of prion strains and their pathogenicity. *Science* **318**: 930–936
- Aguzzi A, Heikenwalder M, Polymenidou M (2007) Insights into prion strains and neurotoxicity. *Nat Rev Mol Cell Biol* **8**: 552–561
- Colby DW, Prusiner SB (2011) Prions. *Cold Spring Harb Perspect Biol* **3**: a006833
- Sturchler-Pierrat C et al (1997) Two amyloid precursor protein transgenic mouse models with Alzheimer disease-like pathology. *Proc Natl Acad Sci USA* **94**: 13287–13292
- Radde R et al (2006) Abeta42-driven cerebral amyloidosis in transgenic mice reveals early and robust pathology. *EMBO Rep* **7**: 940–946
- Aslund A, Herland A, Hammarstrom P, Nilsson KP, Jonsson BH, Inganas O, Konradsson P (2007) Studies of luminescent conjugated polythiophene derivatives: enhanced spectral discrimination of protein conformational states. *Bioconjug Chem* **18**: 1860–1868
- Sigurdsen CJ et al (2007) Prion strain discrimination using luminescent conjugated polymers. *Nat Methods* **4**: 1023–1030
- Nilsson KP, Ikenberg K, Aslund A, Fransson S, Konradsson P, Rocken C, Moch H, Aguzzi A (2010) Structural typing of systemic amyloidoses by luminescent-conjugated polymer spectroscopy. *Am J Pathol* **176**: 563–574
- Eisele YS et al (2009) Induction of cerebral beta-amyloidosis: intracerebral versus systemic Abeta inoculation. *Proc Natl Acad Sci USA* **106**: 12926–12931
- Schmidt M, Sachse C, Richter W, Xu C, Fandrich M, Grigorieff N (2009) Comparison of Alzheimer Abeta(1–40) and Abeta(1–42) amyloid fibrils reveals similar protofilament structures. *Proc Natl Acad Sci USA* **106**: 19813–19818
- Pauwels K et al (2012) Structural basis for increased toxicity of pathological abeta42:abeta40 ratios in Alzheimer disease. *J Biol Chem* **287**: 5650–5660
- Hardy J (1997) The Alzheimer family of diseases: many etiologies, one pathogenesis? *Proc Natl Acad Sci USA* **94**: 2095–2097
- Seilheimer B, Bohrmann B, Bondolfi L, Muller F, Stuber D, Dobeli H (1997) The toxicity of the Alzheimer's beta-amyloid peptide correlates with a distinct fiber morphology. *J Struct Biol* **119**: 59–71
- Yoshiike Y, Chui DH, Akagi T, Tanaka N, Takashima A (2003) Specific compositions of amyloid-beta peptides as the determinant of toxic beta-aggregation. *J Biol Chem* **278**: 23648–23655
- Harmer A et al (2009) Role of amyloid-beta glycine 33 in oligomerization, toxicity, and neuronal plasticity. *J Neurosci* **29**: 7582–7590
- Kuperstein I et al (2010) Neurotoxicity of Alzheimer's disease Abeta peptides is induced by small changes in the Abeta42 to Abeta40 ratio. *EMBO J* **29**: 3408–3420
- Duering M, Grimm MO, Grimm HS, Schroder J, Hartmann T (2005) Mean age of onset in familial Alzheimer's disease is determined by amyloid beta 42. *Neurobiol Aging* **26**: 785–788
- Kumar-Singh S et al (2006) Mean age-of-onset of familial Alzheimer disease caused by presenilin mutations correlates with both increased Abeta42 and decreased Abeta40. *Hum Mutat* **27**: 686–695
- Jarrett JT, Lansbury PT Jr (1993) Seeding 'one-dimensional crystallization' of amyloid: a pathogenic mechanism in Alzheimer's disease and scrapie? *Cell* **73**: 1055–1058
- Eisele YS et al (2010) Peripherally applied Abeta-containing inoculates induce cerebral beta-amyloidosis. *Science* **330**: 980–982